Electron beam welding of 304 stainless steel to QCr0.8 copper alloy with copper filler wire

Bing-gang ZHANG, Jian ZHAO, Xiao-peng LI, Ji-cai FENG

State Key Laboratory of Advanced Welding and Joining, Harbin Institute of Technology, Harbin 150001, China

Abstract: Electron beam welding (EBW) of 304 stainless steel to QCr0.8 copper alloy with copper filler wire was carried out. Orthogonal experiment was performed to investigate the effects of process parameters on the tensile strength of the joints, and the process parameters were optimized. The optimum process parameters are as follows: beam current of 30 mA, welding speed of 100 mm/min, wire feed rate of 1 m/min and beam offset of −0.3 mm. The microstructures of the optimum joint were studied. The results indicate that the weld is mainly composed of dendritic α phase with little globular ε phase, and copper inhomogeneity only occurs at the top of the fusion zone. In addition, a melted region without mixing exists near the weld junction of copper side. This region with a coarser grain size is the weakest section of the joints. It is found that the microhardness of the weld decreases with the increase of the copper content in solid solution. The highest tensile strength of the joint is 276 MPa.

Key words: 304 stainless steel; QCr0.8 copper alloy; electron beam welding; dissimilar joint; mechanical properties

1 Introduction

Welding of dissimilar metal has the advantage to obtain the beneficial properties of two metals or alloys, and thus has received considerable attention in recent years [1,2]. Copper alloys have been widely applied in aerospace, micro-electronics and metallurgy fields due to their excellent performances such as high thermal conductivity, high conductivity and good ductility [3]. However, the application of copper alloy is limited due to its high density and high cost. While stainless steel is a common material with low cost in most industry fields [4,5]. Therefore, partial replacement of copper alloy components by steel can be an attractive way to overcome the difficulty.

However, one of the main problems for copper and steel welding is their great differences between melting temperature and thermal conductivity. Unsymmetrical temperature field will be formed during the welding process. As a result, the grain on the copper side always grows coarse. Another major problem in copper and steel welding is hot cracking in the heat-affected zone (HAZ) of steel due to copper penetration into grain boundaries

of steel [6]. In order to overcome the above problems, copper alloy and steel have been welded by several methods such as arc welding, diffusion bonding, brazing, laser beam welding and electron beam welding (EBW). VELU and BHAT [7] studied the metallurgical and mechanical properties of steel−copper arc welded joint with bronze and nickel-based super-alloy filler materials. No defects could be found in nickel weld but large porosities in bronze weld. Nickel-based materials prefer to joining steel−copper by arc welding. But the characteristic of the arc heat source can cause a relative huge size of HAZ where the grain grows coarse easily. SABETGHADAM et al [8] joined 410 stainless steel with copper by diffusion bonding process using a nickel interlayer. The thickness of the reaction layer increases with rising the temperature. The diffusion transition zone consists of solid solution and (Fe,Ni), (Fe,Cr,Ni), (Fe,Cr) phase. The maximum value of the shear strength is 145 MPa and the hardness at SS−Ni interface is about HV 432. However, the high-temperature residence time stays long so that the copper grain also grows coarse in this process which is almost like brazing process [9]. YAO et al [10] introduced a new joint configuration called scarf joint and kept the beam fixed on the steel

to overcome the high reflectivity of the copper alloy during the laser beam welding. The result showed that the welded joint with lower dilution ratio of copper in the fusion zone (FZ) exhibited excellent tensile strength. MAGNABOSCO et al [11] studied an electron beam welding process between copper plates and three different austenitic stainless steel plates and investigated the morphology, mechanical properties and microstructure of the joints. Nevertheless, the porosities and microfissures could be found in the weld due to the shrinkage of copper and thermal stresses, respectively. As discussed above, the joint with no welding defects and good properties has still not been obtained by welding process under the condition of controlling the size of grain in HAZ near copper side.

EBW is of high energy-density, low heat-input and rapid cooling rate, which is suitable for dissimilar metal welding [12−14]. Besides, EBW with filler wire can greatly reduce the assembly requirement, welding defects and improve the joint properties by modifying the fusion zone composition. Therefore, EBW with filler wire can be taken into account for copper and steel welding in order to obtain good weld appearance and joint properties. It can promote a new effective way for dissimilar metal welding. Although researches on copper alloy and steel joints have been extensively documented, copper alloy and steel welding by EBW with filler wire has been seldom reported.

In this study, the joining of a copper alloy to a stainless steel was conducted by EBW with filler wire. The effects of process parameters on the tensile strength of the joints were studied by orthogonal experiments in order to optimize the welding process. Consequently, both microstructures and mechanical properties of the optimum joint were investigated.

2 Experimental

304 stainless steel and QCr0.8 copper plates with dimensions of 50 mm×25 mm×2.7 mm were selected as the base materials. The optical micrographs of the two base materials are shown in Fig. 1. The copper alloy filler wire with a diameter of 1.2 mm was used as the additional metal. The chemical compositions of the materials are shown in Tables 1−3. The base metals were mechanically and chemically cleaned before welding. Square butt joint configuration was prepared to fabricate the joints. Figure 2 shows the schematic illustration of welding QCr0.8 copper alloy to 304 stainless steel with copper filler wire.

The welding was carried out by electron beam welding equipment with a focal spot radius of about 0.2 mm. The vacuum degree in the experiments was 2.5×10^{-2} Pa and the wire feeding angle was 60°. The
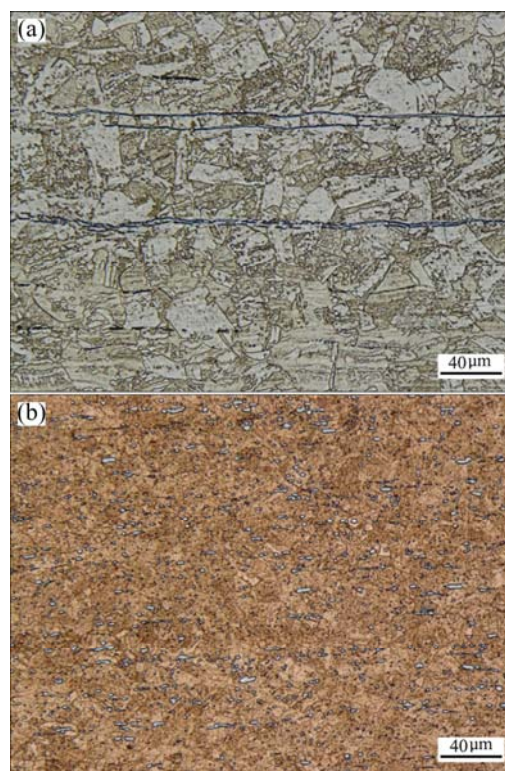
Fig. 1 Optical micrographs of base materials: (a) 304 stainless steel; (b) QCr0.8 copper alloy

Table 1 Chemical composition of 304 stainless steel (mass fraction, %)

C	Si	Mn	P	Cr	Ni	Cu	Fe
0.04	0.60	1.09	0.04	18.3	8.01	0.18	Bal.

Table 2 Chemical composition of QCr0.8 copper alloy (mass fraction, %)

Si	Cr	Ni	Pb	Zn	Mg	Fe	Cu
≤0.02	0.4−0.7	≤0.03	0.005	≤0.015	≤0.002	≤0.05	Bal.

Table 3 Chemical composition of copper filler wire (mass fraction, %)

Si	Mn	P	Sn	Pb	Al	Cu
0.31	0.40	0.05	0.62	0.01	0.002	Bal.
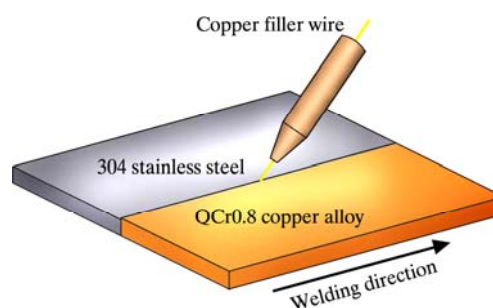
Fig. 2 Schematic illustration of EBW process with filler wire

electron beam was focused on the surface of base metals. The factor−level and orthogonal experimental parameters are presented in Tables 4 and 5, respectively. In beam offset column of Table 5, negative number means the beam focused on steel, zero means the beam focused on the midline and positive number means the beam focused on copper.

Table 4 Factor−level table selected in this study

Level	Factor			
	Beam current/ mA	Welding speed/ (mm·min⁻¹)	Wire feed rate/ (m·min⁻¹)	Beam offset/ mm
1	25	100	1	−0.3
2	30	200	1.6	0
3	35	300	2	0.3

Table 5 Orthogonal experiment parameters used in this study

Sample No.	Beam current/ mA	Welding speed/ (mm·min⁻¹)	Wire feed rate/ (m·min⁻¹)	Beam offset/ mm
1	25	100	1	−0.3
2	25	200	1.6	0
3	25	300	2	0.3
4	30	100	1.6	0.3
5	30	200	2	−0.3
6	30	300	1	0
7	35	100	2	0
8	35	200	1	0.3
9	35	300	1.6	−0.3

The joints were sliced by wire-cut electric discharge machine to prepare the metallographic and tensile specimens. The metallographic specimens were ground by sand paper of 50, 200, 400, 800, 1000 and 1200 grades, then polished and etched with $HCl+FeCl_3+H_2O$ solution. The microstructures were observed by optical microscopy (OLYMPUS SZX12) and scanning electron microscopy (Quanta 200FEG). The microhardness of the joint was evaluated to investigate the microhardness distribution along horizontal direction on the upper and bottom of cross section. The test was carried out by Vickers microhardness tester (HXD−1000TM) at a load of 200 g and a dwell time of 10 s. The tensile test was carried out with the electronic universal material testing machine (Instron 5500R). The displacement velocity of tensile specimens was 3 mm/min. The standard tensile sample for measuring tensile strength was described in details in GB/T+228−2002. Meanwhile, the sample with a width of 4 mm was considered in order to guarantee the uniformity of weld width. Figure 3 shows the schematic

illustration of tensile sample, where L_c, L_t and b are 30, 50 and 2.7 mm, respectively. Before the tensile test, two similar samples were prepared for each joint and both surfaces of the weld were ground to be relatively smooth.
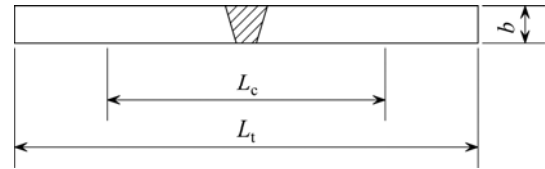
Fig. 3 Schematic illustration of tensile sample

3 Results and discussion

3.1 Effects of process parameters on tensile strength

Table 6 shows the results and range analysis of orthogonal experiment of the joints. In Table 6, the effects of process parameters on the tensile strength can be depicted as follows: beam current > welding speed > wire feed rate > beam offset. The optimum process parameters are beam current of 30 mA, welding speed of 100 mm/min, wire feed rate of 1 m/min and beam offset of −0.3 mm. Figure 4 shows the effects of the process parameters on the tensile strength of the joints. It can be seen from Fig. 4(a) that the tensile strength firstly increases and then decreases with the increase of the beam current. The reason is that the penetration increases with the increase of the beam current. However, when the full penetration is obtained, the grain of copper alloy grows coarse with a further increase of beam current. As shown in Fig. 4(b), the tensile strength decreases

Table 6 Results and range analysis of orthogonal experiment of joints

Joint No.	Beam current/ mA	Welding speed/ (mm·min⁻¹)	Wire feed rate/ (m·min⁻¹)	Beam offset/ mm	Tensile strength/ MPa
1	25	100	1	−0.3	263.81
2	25	200	1.6	0	160.5
3	25	300	2	0.3	138.6
4	30	100	1.6	0.3	260.48
5	30	200	2	−0.3	258.97
6	30	300	1	0	274.02
7	35	100	2	0	257.69
8	35	200	1	0.3	252.89
9	35	300	1.6	−0.3	226.62
K_1	187.64	260.66	263.57	249.80	
K_2	264.49	224.12	215.87	230.74	
K_3	245.73	213.08	218.42	217.32	
R	76.85	47.58	45.15	32.48	
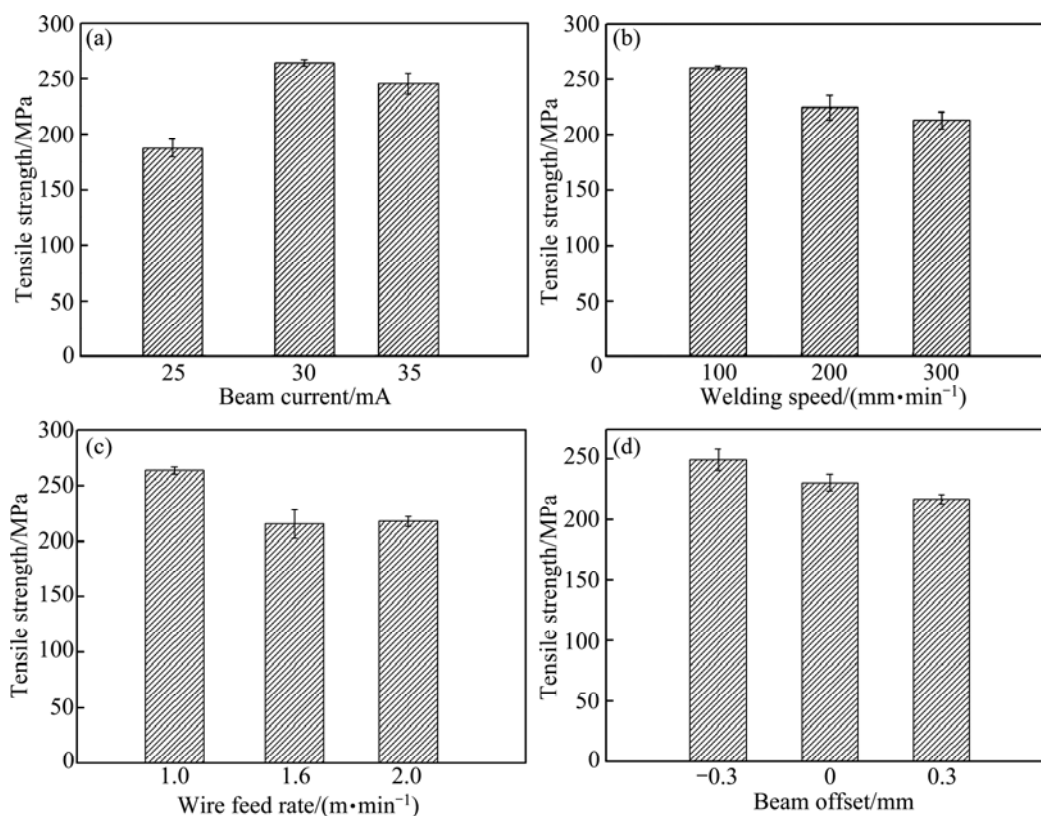
Fig. 4 Effects of process parameters on tensile strength of joints: (a) Beam current; (b) Welding speed; (c) Wire feed rate; (d) Beam offset

gradually with the increase of welding speed. This is because full penetration cannot be obtained by less heat input. The tensile strength decreases with the increase of wire feed rate, as shown in Fig. 4(c). The tensile strength decreases due to stress concentration from bad joint appearance by more feed wire. It can be seen from Fig. 4(d) that the tensile strength decreases with the increase of beam offset. The explanation can be concluded that copper grain grows coarser when the beam is fixed on copper side than that on steel side.

3.2 Microstructure of optimum joint

The optimum joint is obtained at beam current of 30 mA, welding speed of 100 mm/min, wire feed rate of 1 m/min and beam offset of −0.3 mm. The optical macrostructure of typical cross section perpendicular to the welding direction is shown in Fig. 5(a). It can be seen that no macroscopic cracks and pores appear in the joint, which is different from the results in Ref. [11]. There exists acicular phase growing perpendicular to the weld junction near the steel side in Fig. 5(b). Figure 5(c) shows that copper inhomogeneity exists at the top of the FZ due to the rapid cooling rate of EBW process. However, copper inhomogeneity disappears as the depth in the FZ increases, as shown in Fig. 5(d). In addition, fine grain can be found in the weld. This is mainly

attributed to the important role of filler wire playing in cooling down the temperature of the molten pool [15]. Meanwhile, fine grain can be achieved due to the rapid cooling rate as the feature of EBW. A transition region named the melted region without mixing is found near the weld junction of copper side and the grain grows coarse seriously in this zone in Fig. 5(e). In addition, there is less Cr particle distribution in this zone.

The microstructure of the weld was further analyzed by combining Fe−Cu binary phase diagram (Fig. 6) with SEM images (Fig. 7). Figure 6 clearly reveals that Fe−Cu exists in the form of limited solid solubility of Cu in Fe (α phase) and Fe in Cu (ε phase) with no compounds formed. Furthermore, the solubility of Cu in Fe is 11.5%, which is higher than that with 3.5% Fe in Cu. Figure 7(e) shows the EDS spectrum in zone A in Fig. 7(a). Zone A is rich in Fe, Cr and Ni with low Cu content. Therefore, it can be indicated that a little Cu element is distributed into the HAZ of the steel. It can also be seen from Fig. 7(a) that fine δ ferrite grows perpendicularly to the weld junction in the HAZ near the steel side. This is because metatectic transformation occurs between initial δ ferrite and liquid metal firstly, then δ ferrite precipitates from γ austenite. The coarsening of the microstructure is not obvious in HAZ near the steel side. The dark globular phase rich in Fe
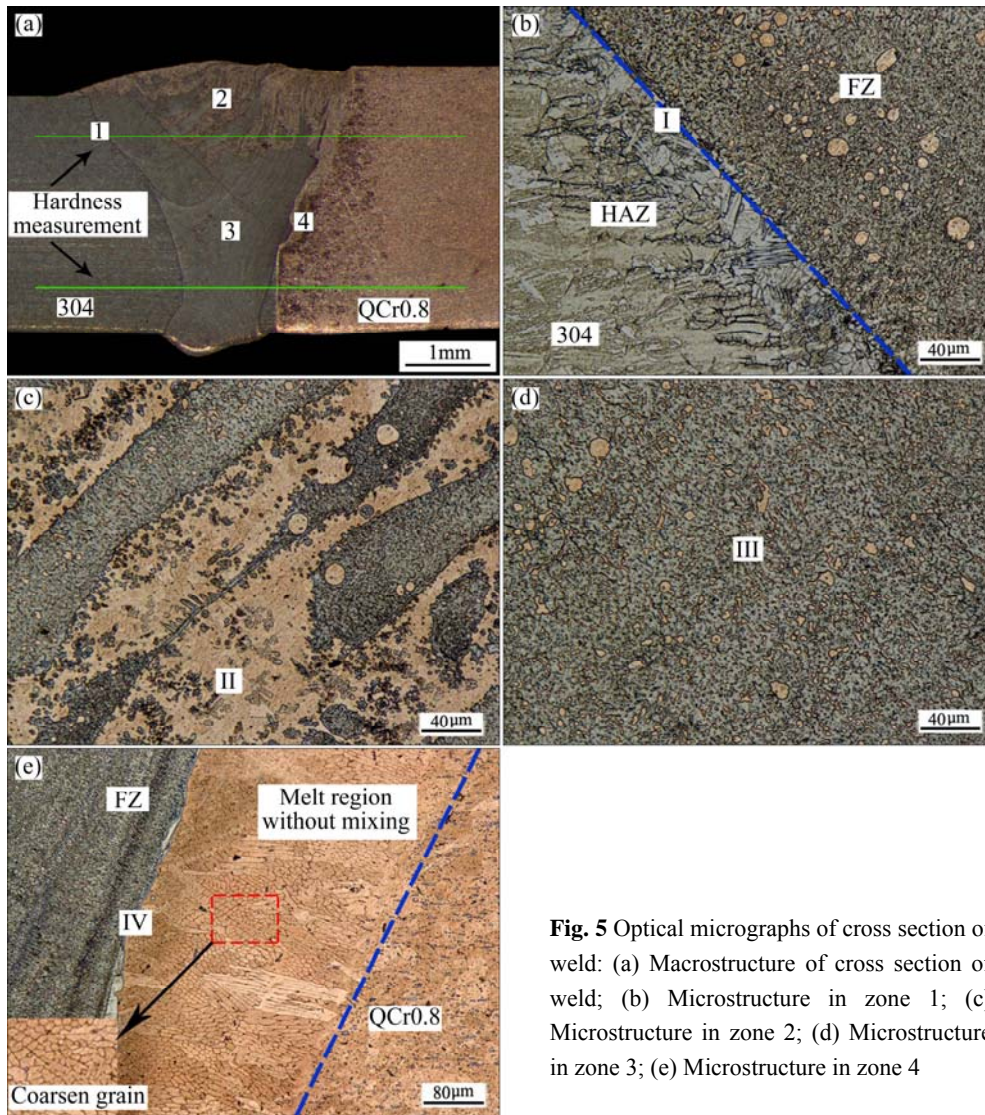
Fig. 5 Optical micrographs of cross section of weld: (a) Macrostructure of cross section of weld; (b) Microstructure in zone 1; (c) Microstructure in zone 2; (d) Microstructure in zone 3; (e) Microstructure in zone 4
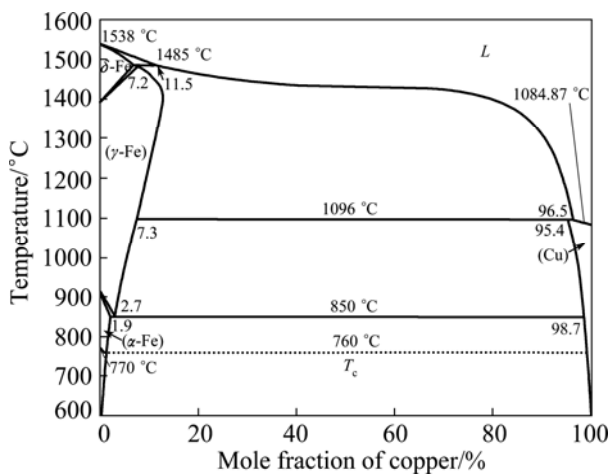
Fig. 6 Fe−Cu binary phase diagram

(Fig. 7(f)) is found to be embedded dispersively in the light zone rich in Cu in Fig. 7(b). The explanation of the result is that the nucleation and growth of Fe in liquid Cu form initially in the form of globular phase owing to the similar temperature gradient at the beginning of the crystallization. Subsequently, fine secondary dendrite grows on the surface of Fe globular phase due to different temperature gradients in the molten pool. Figure 7(g) shows the EDS spectrum in zone C shown in Fig. 7(c). Zone C is rich in Cu with little Fe. This result further proves that Fe with high melting temperature nucleates and grows in the form of dendrite crystal during the crystallization process. One part of liquid Cu dissolves in solidified γ austenite. However, undissolved liquid Cu is repelled by dendritic α phase to the narrow gap of the dendrite forming ε phase. The microstructure is mainly composed of dendritic α phase and little globular ε phase. The inhomogeneity is eliminated because of long high-temperature residence time. In Fig. 7(d), there exists a melted region without mixing near the weld junction of the copper side. The result shows that only a little Fe is distributed into the copper melt zone (Fig. 7(h)) due to the poor fluidity of mushy copper. The grain grows coarse seriously in this area.

3.3 Microhardness

The microhardness distribution on cross section of the weld was measured along the paths marked in Fig. 5(a). The results at the top and the bottom of the weld are shown in Fig. 8(a) and (b), respectively. Comparing the results in Fig. 8(a) with that in Fig. 8(b), it can be concluded that copper inhomogeneity exists at the top of the weld where copper content is higher. Therefore, the microhardness distribution of the top is more unstable than that of the bottom. The results also confirm that the higher microhardness values stay in the zone rich in Fe. On the contrary, lower microhardness values are in the zone rich in Cu. Based on the analysis above, the hardness distribution greatly demonstrates copper inhomogeneity at the top of the weld due to high cooling rate of EBW process.

3.4 Analysis of tensile strength

The tensile strength of copper base material is 363 MPa at room temperature. The tensile strength of the optimum joint can be up to 276 MPa, which is approximately 76% of that of copper base material. The fracture location of the joint occurring in the copper alloy base metal is shown in Fig. 9(a). The toughness fracture can be concluded by obvious characteristic of necking. The fracture mechanism involves two main aspects. On
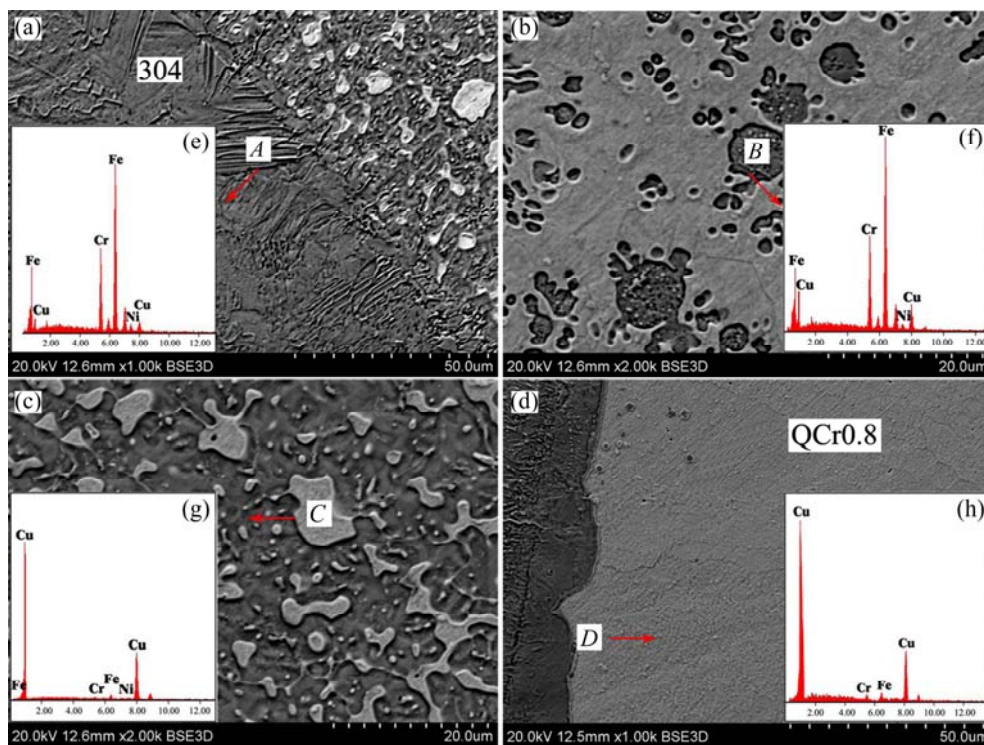
Fig. 7 SEM images (a, b, c, d) of zones in Fig. 5 and EDS spectra (e, f, g, h) of zones in Fig. 7: Zone I; (b) Zone II; (c) Zone III; (d) Zone IV; (e) Zone *A*; (f) Zone *B*; (g) Zone *C*; (h) Zone *D*
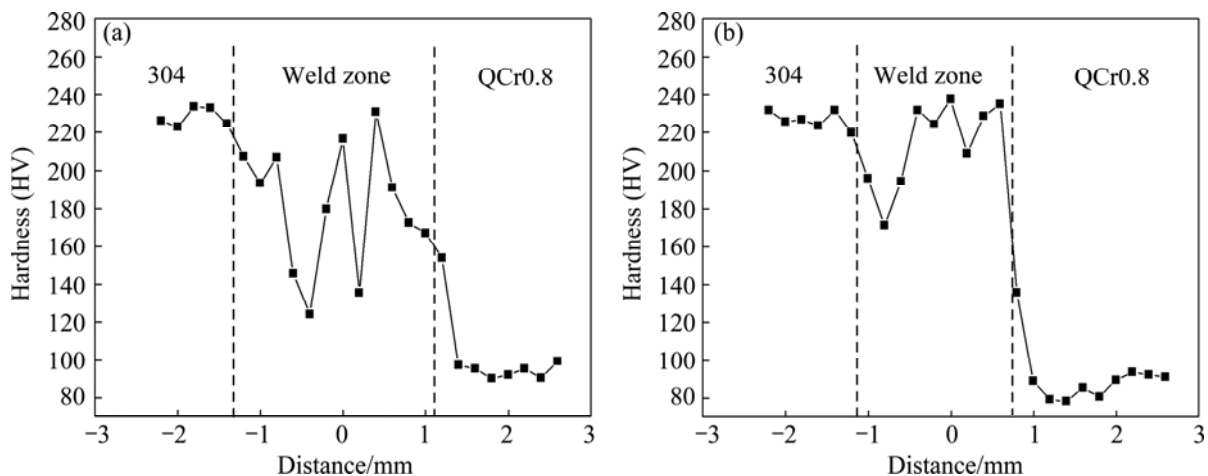
Fig. 8 Microhardness distribution on cross section of weld: (a) At top of weld; (b) At bottom of weld
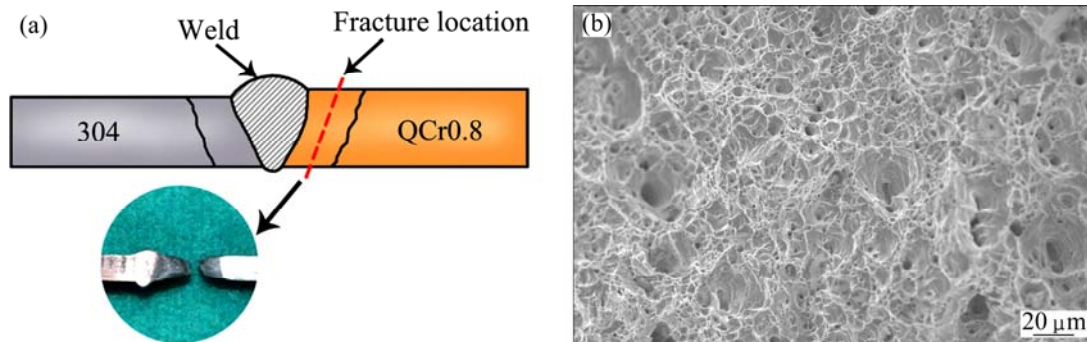
Fig. 9 Fracture mechanism of joint: (a) Fracture location; (b) Morphology of fracture surface

the one hand, most Cr particles distributing in the copper alloy disappear in the melted region without mixing. Therefore, the effect of solution strengthening is weakened. As shown in Fig. 9(b), there are many micro holes in the fracture surface of the joint. The results indicate that the main reason for the formation of micro holes is the dislocation velocity around the second Cr phase particle. These micro holes will grow due to the effect of the external force constantly. The crack can be formed when large numbers of micro holes merge. Subsequently, the fracture occurs. On the other hand, the thermal conductivity between steel and copper alloy is greatly different. The grain grows coarse seriously under the condition of mass of heat focused on the copper alloy, which becomes the weakest section in the joint. Nevertheless, the fine grain can be obtained in the weld by the function of filler wire-induced low temperature in molten pool and rapid cooling rate of EBW process. Thus, the weld with a higher tensile strength is achieved.

4 Conclusions

1) The effect of process parameters on the tensile strength is as follows: beam current > welding speed > wire feed rate > beam offset. The optimum process parameters for EBW of 304 stainless steel to QCr0.8 copper alloy with filler wire are as follows: beam current of 30 mA, welding speed of 100 mm/min, wire feed rate of 1 m/min and beam offset of −0.3 mm.

2) The optimum joint is mainly composed of dendritic α phase with little globular δ phase. Grain grows coarse in the melted region without mixing seriously, which is the weakest section of the joint near the copper side.

3) The microhardness is influenced by the copper content in solution. And the microhardness distribution at the top is more unstable compared with that at the bottom. The tensile strength of the optimum joint is up to 276 MPa, which is approximately 76% of that of copper base material.

References

[1]   SUN Z, KARPPI R. The application of electron beam welding for the joining of dissimilar metals: An overview [J]. Journal of Materials Processing Technology, 1996, 59(3): 257−267.

[2]   WANG Ting, ZHANG Bing-gang, FENG Ji-cai. Influences of different filler metals on electron beam welding of titanium alloy to stainless steel [J]. Transactions of Nonferrous Metals Society of China, 2014, 24(1): 108−114.

[3]   SHIRI S G, NAZARZADEH M, SHARIFITABAR M, AFARANI M S. Gas tungsten arc welding of CP-copper to 304 stainless steel using different filler materials [J]. Transactions of Nonferrous Metals Society of China, 2012, 22(12): 2937−2942.

[4]   YUAN X J, SHENG G M, QIN B, HUANG W Z, ZHOU B. Impulse pressuring diffusion bonding of titanium alloy to stainless steel [J]. Materials Characterization, 2008, 59(7): 930−936.

[5]   YANG J L, LI Y, WANG F, ZHANG Z G, LI S J. New application of stainless steel [J]. Journal of Iron and Steel Research, International, 2006, 13: 62−66.

[6]   MAI T A, SPOWAGE A C. Characterisation of dissimilar joints in laser welding of steel–kovar, copper–steel and copper–aluminium [J]. Materials Science and Engineering A, 2004, 374(1-2): 224−233.

[7]   VELU M, BHAT S. Metallurgical and mechanical examinations of steel–copper joints arc welded using bronze and nickel-base super alloy filler materials [J]. Materials & Design, 2013, 47: 793–809.

[8]   SABETGHADAM H, HANZAKI A Z, ARAEE A. Diffusion bonding of 410 stainless steel to copper using a nickel interlayer [J]. Materials Characterization, 2010, 61(6): 626−634.

[9]   NISHI H, KIKUCHI K. Influence of brazing conditions on the strength of brazed joints of alumina dispersion-strengthened copper to 316 stainless steel [J]. Journal of Nuclear Materials, 1998, 258−263: 281−288.

[10] YAO Cheng-wu, XU Bin-shi, ZHANG Xian-cheng, HUANG Jian, FU Jun, WU Yi-xiong. Interface microstructure and mechanical properties of laser welding copper–steel dissimilar joint [J]. Optics and Lasers in Engineering, 2009, 47(7−8): 807−814.

[11] MAGNABOSCO I, FERRO P, BONOLLO F, ARNBERG L. An investigation of fusion zone microstructures in electron beam welding of copper–stainless steel [J]. Materials Science and Engineering A, 2006, 424(1−2): 163−173.

[12] KIM J, KAWAMURA Y. Electron beam welding of the dissimilar Zr-based bulk metallic glass and Ti metal [J]. Scripta Materialia, 2007, 56(8): 709−712.

[13] WANG Ting, ZHANG Bing-gang, CHEN Guo-qing, FENG Ji-cai, TANG Qi. Electron beam welding of Ti-15-3 titanium alloy to 304 stainless steel with copper interlayer sheet [J]. Transactions of

Nonferrous Metals Society of China, 2010, 20(10): 1829−1834.

[14] CHEN Guo-qing, ZHANG Bing-gang, LIU Wei, FENG Ji-cai. Influence of electron-beam superposition welding on intermetallic layer of Cu/Ti joint [J]. Transactions of Nonferrous Metals Society of

China, 2012, 22(10): 2416−2420.

[15] LIU Li-ming, DONG Chang-fu. Gas tungsten-arc filler welding of AZ31 magnesium alloy [J]. Materials Letters, 2006, 60(17−18): 2194−2197.

304 不锈钢与 QCr0.8 铬青铜填加
铜焊丝的电子束焊接

张秉刚, 赵 健, 李晓鹏, 冯吉才

哈尔滨工业大学 先进焊接与连接国家重点实验室，哈尔滨 150001

摘 要：采用填铜焊丝对 304 不锈钢与 QCr0.8 铬青铜进行电子束焊接。采用正交试验法研究不同工艺参数对焊接接头抗拉强度的影响，并对焊接工艺参数进行优化。优化工艺参数如下：束流 30 mA，焊接速度 100 mm/min，送丝速度 1 m/min，束偏移量−0.3 mm。对优化后接头组织的分析结果表明，焊缝主要由树枝状 α 相与少量球形 ε 相组成；仅在焊缝区的上部出现铜的混合不均匀；而在铜侧熔合线附近存在一个铜的熔化但未混合区，该区域晶粒长大严重，是接头的最薄弱区。显微硬度测试结果显示，焊缝硬度随固溶体中铜含量的增加而减小。接头的最高抗拉强度为 276 MPa。

关键词：304 不锈钢；QCr0.8 铬青铜；电子束焊接；异种接头；力学性能

(Edited by Wei-ping CHEN)